



Field measurements of horizontal forward motion velocities of terrestrial dust devils: Towards a proxy for ambient winds on Mars and Earth

M.R. Balme^{a,b,*}, A. Pathare^a, S.M. Metzger^a, M.C. Towner^c, S.R. Lewis^b, A. Spiga^d, L.K. Fenton^e, N.O. Renno^f, H.M. Elliott^f, F.A. Saca^f, T.I. Michaels^g, P. Russell^h, J. Verdascaⁱ

^a Planetary Science Institute, 1700 E Fort Lowell Rd., Suite 106, Tucson, AZ 85719, USA

^b Department of Physical Sciences, The Open University, Walton Hall, Milton Keynes MK7 6AA, UK

^c Applied Geology Department, Curtin University of Technology, GPO Box U1987, Perth, Western Australia 6845, Australia

^d Laboratoire de Météorologie Dynamique, Université Pierre et Marie Curie, Paris, France

^e Carl Sagan Center at the SETI Institute, 189 Bernardo Ave., Suite 100, Mountain View, CA 94043, USA

^f Department of Atmospheric, Oceanic and Space Sciences, Space Research Building, University of Michigan, 2455 Hayward St., Ann Arbor, MI 48109-2143, USA

^g Southwest Research Institute, 1050 Walnut St., Suite 400, Boulder, CO 80302, USA

^h Center for Earth and Planetary Studies, Smithsonian Institution, PO Box 37012, National Air and Space Museum, MRC 315, Washington, DC 20013-7012, USA

ⁱ Centro de Astrobiología (CSIC/INTA), Instituto Nacional de Técnica Aeroespacial, Ctra de Torrejón a Ajalvir, km 4, 28850 Torrejón de Ardoz, Madrid, Spain

ARTICLE INFO

Article history:

Received 7 June 2012

Revised 11 August 2012

Accepted 14 August 2012

Available online 4 September 2012

Keywords:

Mars, Atmosphere

Earth

Mars

ABSTRACT

Dust devils – convective vortices made visible by the dust and debris they entrain – are common in arid environments and have been observed on Earth and Mars. Martian dust devils have been identified both in images taken at the surface and in remote sensing observations from orbiting spacecraft. Observations from landing craft and orbiting instruments have allowed the dust devil translational forward motion (ground velocity) to be calculated, but it is unclear how these velocities relate to the local ambient wind conditions, for (i) only model wind speeds are generally available for Mars, and (ii) on Earth only anecdotal evidence exists that compares dust devil ground velocity with ambient wind velocity. If dust devil ground velocity can be reliably correlated to the ambient wind regime, observations of dust devils could provide a proxy for wind speed and direction measurements on Mars. Hence, dust devil ground velocities could be used to probe the circulation of the martian boundary layer and help constrain climate models or assess the safety of future landing sites.

We present results from a field study of terrestrial dust devils performed in the southwest USA in which we measured dust devil horizontal velocity as a function of ambient wind velocity. We acquired stereo images of more than a 100 active dust devils and recorded multiple size and position measurements for each dust devil. We used these data to calculate dust devil translational velocity. The dust devils were within a study area bounded by 10 m high meteorology towers such that dust devil speed and direction could be correlated with the local ambient wind speed and direction measurements.

Daily (10:00–16:00 local time) and 2-h averaged dust devil ground speeds correlate well with ambient wind speeds averaged over the same period. Unsurprisingly, individual measurements of dust devil ground speed match instantaneous measurements of ambient wind speed more poorly; a 20-min smoothing window applied to the ambient wind speed data improves the correlation. In general, dust devils travel 10–20% faster than ambient wind speed measured at 10 m height, suggesting that their ground speeds are representative of the boundary layer winds a few tens of meters above ground level. Dust devil ground motion direction closely matches the measured ambient wind direction.

The link between ambient winds and dust devil ground velocity demonstrated here suggests that a similar one should apply on Mars. Determining the details of the martian relationship between dust devil ground velocity and ambient wind velocity might require new in situ or modelling studies but, if completed successfully, would provide a quantitative means of measuring wind velocities on Mars that would otherwise be impossible to obtain.

© 2012 Elsevier Inc. All rights reserved.

* Corresponding author at: Planetary Science Institute, 1700 E Fort Lowell Rd., Suite 106, Tucson, AZ 85719, USA.

E-mail address: mbalme@psi.edu (M.R. Balme).

1. Introduction

Dust devils are convective vortices carrying dust and debris entrained from the surface (e.g., Balme and Greeley, 2006). They are powered by solar insolation and form most commonly in hot, arid environments where there are strong vertical temperature gradients (Renno et al., 1998). Dust devils are not limited to the Earth, and have been identified on Mars from orbit in both high and low resolution imaging data (e.g., Thomas and Gierasch, 1985; Malin and Edgett, 2001; Fisher et al., 2005; Cantor et al., 2006; Stanzel et al., 2008; Towner, 2009) and from the surface in both images and meteorology data (e.g., Ryan and Lucich, 1983; Metzger et al., 1999; Ferri et al., 2003; Greeley et al., 2006; Ellehoj et al., 2010). Martian dust devils might be responsible for the persistent dustiness of the martian atmosphere especially in the northern hemisphere summer when weather systems are generally weaker (Newman et al., 2002), as their ability to lift dust could be enhanced both by the local wind shear and their low-pressure cores which could act to ‘suck-up’ material as they move across the surface (Greeley et al., 2003; Balme and Hagermann, 2006).

Although dust devils are highly localized phenomena, they form within regional circulations and, as such, may reflect the forces operating in that larger context. If so, their behavior might provide an opportunity to recognize general ambient conditions when no other means are available. The work presented here describes the measurement of the horizontal forward motion of dust devils and the comparison of these data with simultaneous local meteorology measurements. We use the term ‘ground velocity’ to refer to the speed and direction the dust devils move horizontally across the surface, and use ‘ground speed’ or ‘ground direction’ to refer to magnitude and direction of the velocity. Obtaining good measurements of dust devil forward motion is important because it provides information about how dust devils fit into local and regional circulation patterns. Hence, there is a need for a large number of precise measurements linked closely with reliable ambient meteorology data. The main aim of this work is therefore to determine whether measurements of the ground velocity of dust devils can be used as a proxy for ambient wind speed. Given the very limited number of measurements of near-surface wind speed and direction that exist for Mars, any such information would be of value for understanding wind circulation on Mars.

2. Previous work

The forward motions of terrestrial dust devils have not been studied in detail, with most such measurements being little more than estimates. Those measurements that were reliably made are limited in dataset size, are sometimes contradictory, or were not collected with concurrent local meteorology measurements. For example, Flower (1936) observed dust devils ranging in diameter from less than 2 m to greater than 50 m and found that tall and moderately wide dust devils moved fastest, and estimated speeds of up to about 10 ms^{-1} . Crozier (1970) used stereo imaging and also found that dust devils of several tens of meters in diameter had ground velocities of about 10 ms^{-1} and followed ambient wind directions. In contrast, Snow and McClelland (1990) suggested that ground speeds were more commonly around 4 ms^{-1} , and suggested that speeds greater than 11 ms^{-1} were probably measurement errors.

Dust devils appear to travel in approximately the direction of the prevailing winds (Ives, 1947; Williams, 1948; Sinclair, 1969), but whether their ground speeds correlate with ambient wind speed is less well understood. Flower (1936) and Crozier (1970) both found that the motions of dust devils approximated the ambient winds, both in terms of direction and magnitude, but Snow and

McClelland (1990) found that ambient wind speeds (measured at 10 m height) were usually at least twice as large as dust devil translation speeds. However, very little detail is available about how many of these measurements were made, or how close to each dust devil the winds were recorded. Crozier’s measurements, for example, were based only on subjective estimates of wind speed.

The formation of convective vortices (i.e. vortices equivalent to dust devils but not necessarily dust-loaded) has been demonstrated in high-resolution models of planetary atmospheres (e.g., Toigo et al., 2003; Kanak, 2005) but horizontal ground motion often has not been explicitly described. Toigo et al. (2003) found that in both high and low ambient wind experiments under martian conditions, convective vortices move with the cellular convection circulation within which they are embedded. In simulations aimed at exploring dust lifting by convective vortices on Mars, Michaels (2006) describe a dust devil travelling with the same horizontal ground velocity ($\sim 2 \text{ ms}^{-1}$, west to east) as the ambient wind velocity at 2 m above ground level.

The ground velocity of dust devils on Mars has also been measured, with these data being determined by time-sequence imaging either from orbit (Stanzel et al., 2006, 2008; Reiss et al., 2011) or from the surface (e.g., Metzger et al., 1999; Ferri et al., 2003; Greeley et al., 2006, 2010). In many ways, the remote sensing data are more reliable than terrestrial field or Mars surface data, because both dust devil position and time of image acquisition can be measured more accurately, and hence ground velocity derived reliably. This means that there are potentially a large number of measurements of dust devil ground velocity that can be made, based on the large number of imaging data that exist for the martian surface. In contrast, there are currently few meteorology data from Mars, as only the Viking Lander (and to some extent the Phoenix and Mars Pathfinder Landers) had the ability to measure wind direction and speed on the surface, meaning that numerical modeling often is used to infer the near-surface wind field on Mars.

The most reliable data on martian dust devil ground velocity come from the High Resolution Stereo Camera, or HRSC (Neukum and Jaumann, 2004) instrument onboard the ESA Mars Express spacecraft. This detector has nine channels which each collect images of the same area of the surface. The acquisitions of these images are separated in time by a few tens of seconds, allowing the progress of dust devils to be observed across the surface during these intervals. Stanzel et al. (2006, 2008) and Reiss et al. (2011) used this technique to determine the forward motion of dust devils. Most of the dust devils analyzed were large – of the order of hundreds of meters in diameter, reflecting the $\sim 25 \text{ m}$ pixel size of HRSC stereo channel images – compared with observations of dust devils from landing craft, which analyzed much smaller dust devils (e.g., Greeley et al., 2010).

Stanzel et al. (2008) provide the largest data set, reporting 205 dust devils from 23 HRSC image ‘triplets’ each comprising two stereo images and one nadir image. They found traverse speeds of individual dust devils that ranged from a few ms^{-1} to nearly 60 ms^{-1} . The ground speeds of the dust devils Stanzel et al. (2008) describe are fairly consistent within image triplets. For the 17 image triplets (or sometimes doublets) that contain more than two dust devils, the standard deviation of the ground speed is usually less than a third of the mean value, even though the mean ground speed ranges from less than 4 ms^{-1} to nearly 30 ms^{-1} . Greeley et al. (2010) measured the ground speeds of about 500 dust devils using surface observations from the Mars Exploration Rover, *Spirit*. They found maximum speeds of nearly 30 ms^{-1} , but their measurements indicated ground speeds of dust devils were mostly less than 10 ms^{-1} . Interestingly, Greeley et al. found that smaller dust devils travelled faster, although they acknowledge that there is a large amount of scatter in their data.

If the ground velocity of dust devils can be shown to correlate well with local wind vectors, then martian dust devils can serve as complements or alternatives to field anemometers and wind vanes, providing measurements of wind speed and direction in the absence of near-surface meteorology instruments. These data would further constrain climate models and provide better knowledge of the wind environment in terms of landing site selection.

Before measurements of martian dust devil forward motions can be used in this way, two questions must be answered: (i) do dust devils move with the local wind in a predictable fashion? (ii) if so, what expression can be derived that links dust devil forward motion to the local winds? At present, only terrestrial field studies can answer these questions. This paper presents a method for measuring size and location of dust devils based on stereo imaging, and reports data from two field seasons spent studying dust devils in Arizona and Nevada in the southwest USA. Measurements from more than a 100 individual dust devils are presented here. We use these data to determine the location of dust devils and use multiple measurements of individual dust devils to calculate their ground velocities. Concurrently, at each field site we used a network of meteorology masts to define the local wind regime. Hence we are able to correlate the forward motion of each dust devil with the local winds at the time it was active.

3. Field sites

In 2009 we conducted dust devil surveys in two field sites (Fig. 1) in the southwestern United States: Eloy, Arizona (centered at 32.665°N, –111.546°E) and Eldorado Valley, Nevada (centered at 35.839°N, –114.963°E). In 2010 we conducted a repeat survey in Eldorado Valley. Both these locations have been used previously as dust devil study-sites and are well-characterized (e.g., Metzger, 1999; Balme et al., 2003; Renno et al., 2004). The Eloy site is located approximately midway between the cities of Tucson and Phoenix and consists of a mixture of cultivated agricultural lands and arid desert terrain, including limited shrub cover. The Eloy site lies at an elevation of about 500 m, and is a very flat site, with no significant hills within about 10 km. The Eldorado Valley site, about 30 km southeast of Las Vegas, is a dry playa lake within basin and range terrain, surrounded by low hills and alluvial fans, and has little to no vegetation. The Eldorado Valley site lies at an elevation of about 500 m, and sits in a basin ringed by terrain with elevations of ~1000 m within 10 km of the site.

For each site, study areas were defined with the aim of recording all dust devils that formed within, or crossed through, these areas. The study area boundaries were mapped using a handheld Global Positioning System (GPS) unit. For Eloy, the boundary of

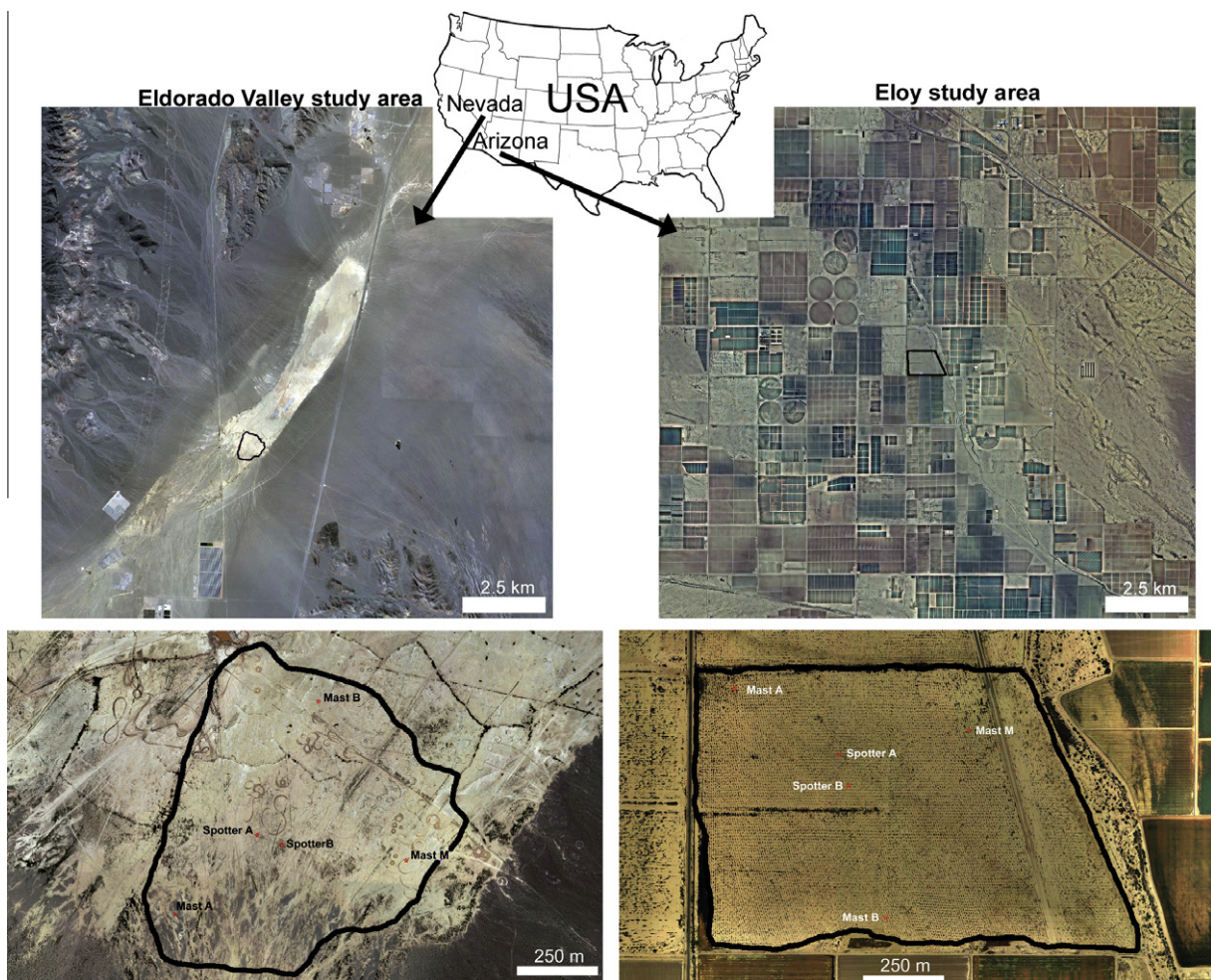


Fig. 1. Locations of field sites. The Eldorado site (left hand side of image) is located in the southern part of a playa lake that sits in turn within a basin. The precise boundary of the study area is shown by the black outline. The close-up view (bottom left) shows the study area outline, the positions of the three meteorology masts (designated A, B and M), and the positions of the two spotter stations (A and B). The southern part of the study area contains the distal end of alluvial fan/debris flows, but otherwise the surface is fairly homogeneous. The Eloy site (right) is within very flat agricultural land and, apart from the light-aircraft runway in the east is extremely homogeneous. Image base maps are from the ESRI ArcGIS online imaging service. Image credit ESRI; i-cubed.

the study site was defined by field margins, but for Eldorado, a combination of surface textures and lines of shrubs was used. High visibility surveying tape (tied to stakes, flags or individual bushes) was further used to define areas where the boundary was unclear. The Eloy survey area was equal to 0.83 km²; the Eldorado survey area was 0.55 km². The clear boundaries along the rectangular Eloy tract permitted a larger survey region. Three meteorology masts were deployed at each study area, forming an approximately equilateral triangle within the study area boundary (see Fig. 1). For Eldorado Valley, the same mast positions were used in 2009 and 2010.

4. Approach

4.1. Overview

To obtain the ground velocity of a dust devil, accurate measurements of its position must be made at least twice during its life-span. In this study, the size and position of the dust devils were obtained using a stereo camera system consisting of two imaging 'spotter' stations at the center of the study area (see Fig. 1). This allowed quantitative measurements of the bearing and angular width of the dust devils to be made from each station. The two imaging stations were each attended by a spotter team member tasked with taking simultaneous photographs of the dust devils.

Four requirements were identified for the approach: (1) The position of the dust devil should be measured to an angular precision of $\sim 0.1^\circ$ of arc to allow ~ 1 m diameter dust devils to be resolved at ~ 500 m. (2) Any instrumentation should be robust and easily replaced. The likelihood of damage to sensitive equipment was deemed high, so it had to be able to survive the strong winds, intense activity and the hot and dusty environment. (3) Previous experience has shown that dust devils can travel at several meters per second and that multiple dust devils often occur in the same local area at once. Hence, simplicity and rapidity of use in the field was vital to make multiple measurements of dust devils. (4) Cost effectiveness.

To meet these requirements we used 'point and shoot' weather-proof 6 megapixel digital cameras with user-definable optical zoom and exposure capabilities. The cameras were each mounted on a sturdy tripod with a head free to rotate around a vertical axis. In 2009 we used a zoom level of 5.6 \times , equating to a focal length of 20.4 mm and a field of view per frame of $\sim 17^\circ$. In 2010 we used a lower zoom factor with a field of view of $\sim 45^\circ$ because results from the previous year had demonstrated that this would have significant advantages (i.e. much easier targeting for the spotter and the ability to photograph nearer dust devils without them overlapping the edge of the image) and few disadvantages (we found that the limiting factor in pinpointing dust devils within the image was not a function of angular resolution, but more a lack of contrast for distant, small dust devils). In 2009 the zoom level and field of view gave >20 pixels per 0.1° of arc; in 2010 this was reduced to >7 pixels per 0.1° .

The parameters required to calculate the size and location of the dust devils are: the locations of the cameras, the bearing of the dust devil from each camera at that time, and the angle subtended by the dust devil as seen from the camera. For each location, GPS was used to determine the position of the imaging station, giving a horizontal precision of about 0.5 m. To determine the bearing and angular width of each dust devil, we first constructed a 360 $^\circ$ panorama image from each camera location, to which all subsequent photographs could then be referenced, and the position of dust devils within the frame measured.

An advantage of using this system of central cameras over, for example, fixed inward looking cameras at the edge of the study area is that a larger area can be covered and smaller dust devils

seen. The disadvantage of this approach was that it required at least two spotters to be in the field for the duration of the study. This requirement was not a serious limitation, and in some senses was an advantage, for a larger team meant that dust devils were more quickly identified, and note-taking and documentation of many of the characteristics of the dust devils were more easily accomplished than if a single person was performing the study.

Several other methods were considered in the planning stages of this project. The first option was to use multiple cameras with a remotely controlled shutter operated by a single person. However, this system would still have required two operators as the cameras had to be pointed separately and would have required more costly – and more easily damaged – cameras for it to be achievable. We also considered using two upward looking cameras with fisheye lenses that could be triggered automatically or remotely. This system suffered from a lack of image resolution, and thus to mitigate this many cameras would have had to be used. This was considered too expensive and complicated. Finally, we considered using twin cameras with built in GPS/pointing capability, but did not find cameras with accurate enough pointing capabilities to be able to measure the bearing of a dust devil to the required 0.1° . The simplest and, importantly, most robust approach was therefore to use two cameras and two operators and to later register the images to the background panorama.

4.2. Field methods

The survey was performed by at least two (and almost always three) observers positioned at the spotter stations at the center of the study area (Fig. 2). For each dust devil observed within the study area, two of the spotters photographed the vortex as it moved across the study area while a third (dubbed the 'surveyor') recorded the qualitative size, duration and dustiness, as well as noting the dust devil's approximate path on a map (for a description of the approach see Pathare et al., 2010). Whenever possible, the surveyor was in a raised position, standing in the bed of a pick-up truck at the center of the survey region, and was tasked with coordinating the survey and determining whether each dust devil was within or outside the defined study area. This allowed the

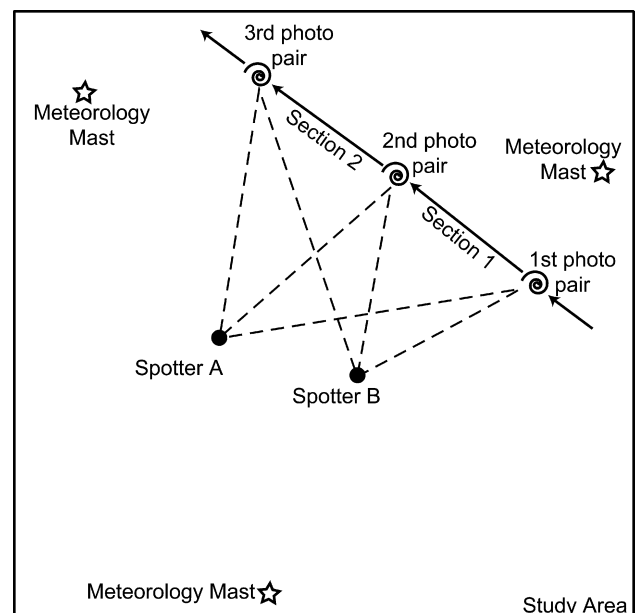


Fig. 2. Sketch showing location of spotter camera stations in relation to a passing dust devil and the three meteorology masts. In this example, three photographic pairs were acquired, allowing three measurements of dust devil size and position, and two measurements (Sections 1 and 2) of dust devil ground velocity.

two spotters to concentrate on accurately taking simultaneous images of the dust devils without being hampered by data-recording tasks. Prior to the beginning of the survey a series of panorama images, each overlapping by half a field of view from the previous, were taken from each imaging station. These used the same camera settings as the spotting images and were taken from the same position and with the same cameras. All camera clocks were updated daily to GPS time to ensure that the time of each photograph was recorded accurately.

For most dust devils recorded by the spotters at least one pair (and often several) of simultaneous photographs were taken. The same positions of the spotter camera stations were kept throughout the field campaigns. The spotters were in communication by radio, allowing the dust devils to be photographed simultaneously when commanded by the lead spotter. Each dust devil was given an identification code by the surveyor as it was observed and the image number and time of each photograph was recorded separately by each camera operator. At the end of each day, the individual images were filed by dust devil ID number and stored for later processing.

Three meteorology masts were deployed in this study. Two 10 m masts (denoted A and B) were used, each instrumented by five cup anemometers, three temperature sensors, one barometer and a single wind vane at 10 m. Data were logged at one second intervals, recorded on Campbell CR-1000 data loggers, and downloaded at the end of each day. Only the results from the anemometer and vane set at 10 m height will be discussed here – the rest of the instrumentation, and the results from the third mast, are of relevance to other aspects of the larger project to study dust devils in this area. The measurements of wind speed and direction from masts A and B were never further than ~500 m from the dust devils studied.

4.3. Post-field methods

After the field campaign, a Geographical Information Systems (GIS) technique was used to analyse the imaging data. This allowed the angular position and width of each dust devil to be determined and metadata (such as dust devil ID number, date, and time) attached. The method can be split into four main steps (Fig. 3):

- (1) Pairs of images (one from each spotter) that contain dust devils were identified and imported into a 'parallax' GIS (with a cylindrical projection) and referenced against the background panorama. A separate GIS was built for each spotter position and for each study area and observation year.
- (2) Within the parallax GIS, each dust devil was carefully digitized with a simple horizontal line across its width. The azimuth of the start point and center point of that line were calculated in the GIS and exported to pairs of data files (one for each imaging station).
- (3) Using simple geometry, the pairs of angular width/azimuth data were converted into position and diameter data for each dust devil observation, giving a single dataset of location, size and time (of observation) records.
- (4) These data were imported into a new 'map' GIS and displayed on a map of the study region in a Universal Transverse Mercator (UTM) projection. In the map GIS, each dust devil is represented by a circle showing its diameter and position. Where multiple observations of a dust devil were made, the map GIS contains several such circles for a single dust devil. These are connected by vector objects that include metadata describing the length of that vector, its

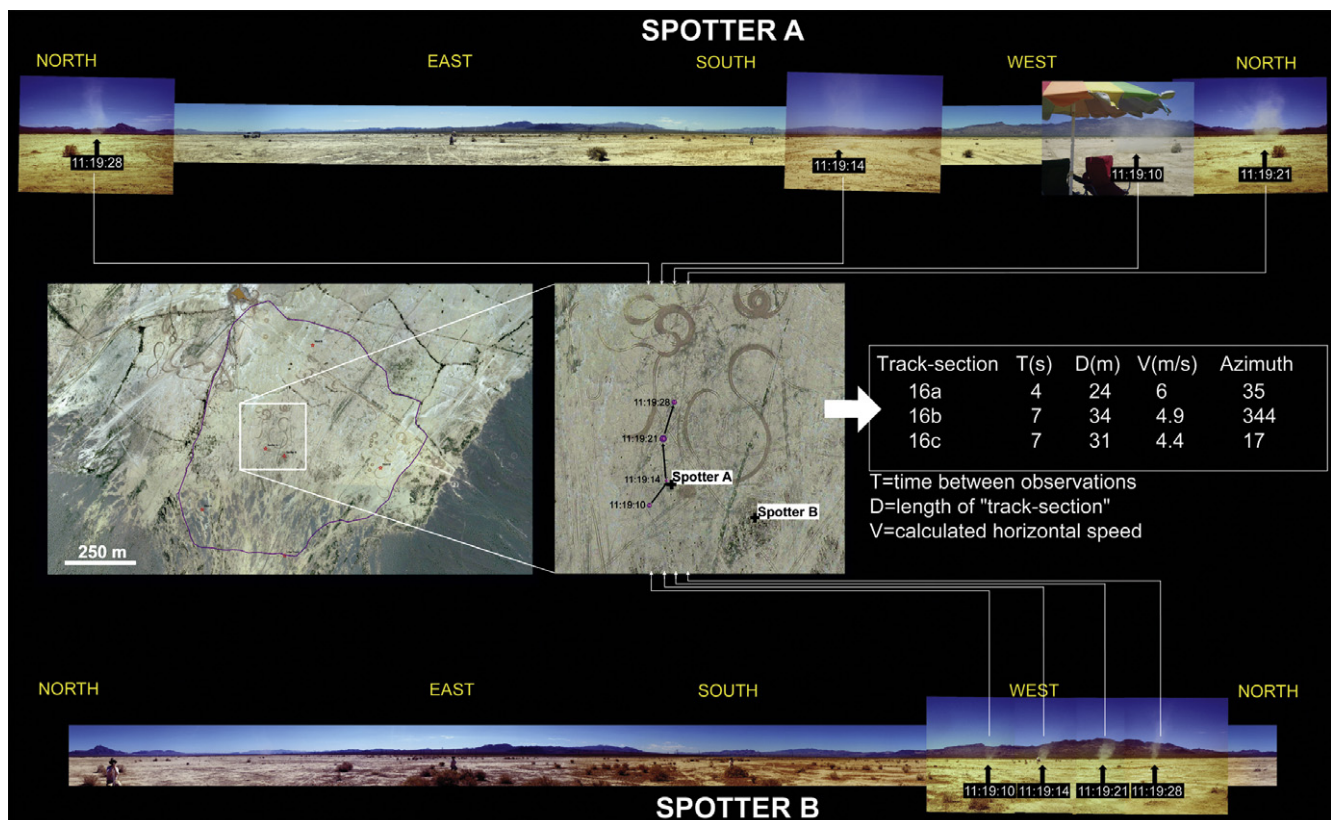


Fig. 3. Diagram showing the image processing pipeline required to obtain size/position measurements of dust devils. In the first step, multiple photographs of the same dust devil are plotted against the background panorama, for both Spotter A (top) and B (bottom). The angular size and azimuth from each spotter are converted into position and diameter measurements and displayed on a map of the study area (center). From this map, velocity measurements can be extracted, knowing the time each image was taken.

projected azimuth, the length of time between observations and the other metadata describing that dust devil. The vector data were then exported for comparison with local meteorology.

The background panoramas for step 1 were created by stitching the overlapping panorama images together using the software tool 'Hugin' and generated using a cylindrical projection. The Hugin tool is a free graphical interface for the 'Panorama Tools' software suite (<http://panotools.sourceforge.net/>). This maintains a weblink but removes the reference. These panoramas were tested and calibrated by measuring the azimuthal position of terrain features in the mid-field (e.g. electrical poles, trees, houses, etc.) and far-field (mountain peaks, distant buildings, etc.) in the panoramas and comparing these with the bearings of the same features in high resolution aerial remote sensing data, or from field GPS measurements. The panoramas proved to be robust, with the azimuths calculated from the panoramas for all the calibration points matching their true bearings to $\pm 0.1^\circ$.

To reference the dust devil images against the background panorama, each dust devil image was assigned a GIS world file that described its resolution and position (initially all were assigned a default position of due north) and a projection to match the panorama. Then, these images were overlain by hand on the panorama using the ArcInfo *georeferencing* tool. For most cases only two tie-points were used, which, coupled with a linear first-order fit, allowed simple scaling, translation and rotation of the image to fit. In all cases the tie-points used were selected immediately on either side of the dust devil. It should be noted that neither vertical distortions nor distortions of the image away from the dust devil itself were considered significant – the sole requirement was to ensure that the width of the dust devil itself was correctly mapped onto the background panorama.

Following image referencing, each dust devil was digitized using a simple horizontal line shapefile (a GIS vector data format). Additional data including dust devil ID number, image time and date were also stored as the dust devil was digitized. For each dust devil, two digitized lines were drawn: one from the spotter A image referenced to the spotter A panorama and one from the Spotter B image referenced to the Spotter B panorama. From these shapefiles the start point and center point of each line were then extracted and exported to a calculation spreadsheet.

For the many columnar and well-defined dust devils photographed, digitizing was straightforward. However, natural dust devils are not always simple columns of dust – they are often disordered, v-shaped, comprise multiple interior rotating columns, or in other ways are complex and variable over their duration. For these we developed additional processing steps and guidelines. For diffuse dust devils image processing was sometimes needed to reveal them or determine their widths. This was performed within the GIS using either a simple 'min-max' level stretch, in which the range of the brightness levels of the input image was mapped onto the full range of levels available in the output image, or a 'standard deviations' stretch wherein the intensity range of the output image was created from different central sections of the full range of the input image levels, thereby improving the contrast of different parts of the levels range. Dust devils that were too faint for their shape to be accurately defined were excluded from the study. For complex dust devils, the following guidelines were developed to ensure internal consistency within the data set. For dust devils comprising multiple subsidiary vortices within a poorly dust-loaded envelope we measured the whole system; in cases where dust devils had a diffuse outer column surrounding a well-defined central column, we measured the outer column width, and where dust devils had v-shaped columns we defined the width as the point at which the v-shaped column transitioned

into a more vertical one. When dust devils had columns that were at an angle to the surface (as is often the case) we defined the width as usual but placed the center point where the dust devil intersected the ground. Although it is virtually impossible to define the range of dust devil morphologies in any simple way and in some cases arbitrary decisions regarding the positioning of dust devil edges had to be made, we endeavored to be consistent throughout the study.

When the size and position of each dust devil had been extracted, the diameters of each dust devil, as measured from the two different imaging stations, were compared. Those pairs showing high discrepancies (more than 15%) were double-checked in the parallax GIS. Differences were sometimes assigned to digitizing error and corrected, but in some examples the dust devils did appear to be wider in one spotter's image than another. This is unsurprising given that the spotters observed the dust devils from two different angles and that the geometrical solution assumes that all dust devils are simple, solid cylinders. In reality, of course, dust devils are not always cylindrical and the effects of both this and lighting effects altering the perceived shape of a dust devil were impossible to account for. Furthermore, many dust devils demonstrate variable dimensions over their lifetime.

Although discrepancies in the measurements arising from the complex nature of the dust devils themselves are difficult to quantify, errors inherent in the technique are not. We propagated estimated measurement errors to create errors in the final position and diameter of each dust devil. The dominant source of error in position is the uncertainty in the selection of the center point of the dust devil. This could arise from two main sources: (i) camera pointing error, including panorama inaccuracy and referencing accuracy, and (ii) phenomenon-intrinsic 'error' including digitizing difficulties and asymmetry of dust devil columns. Error in the measured pointing azimuth becomes large when the parallax angle becomes small (i.e. when the bearing of the dust devil is similar from both spotters). Hence, error in the measured range becomes high when (i) the dust devils are aligned with the spotters along the baseline of the camera survey and (ii) when the distance to the dust devil becomes large. To display this error, the propagated error in range from each spotter was determined to create four points in space around the position of the dust devil. An ellipse was then fitted to these points to give an estimate of the spatial uncertainty in the position of the centroid of each dust devil. Fig. 4 demonstrates how most of the uncertainty in position is radial with respect to the observers.

To convert position measurements into ground velocity vectors, UTM map-projected data were used. For each dust devil that had been photographed multiple times the distance and time between successive positions was extracted from the GIS to give the speed and direction of travel. We were able to extract several horizontal motion vectors for most dust devils. The positional error ellipses defined above were used to give an estimate of the maximum and minimum distance the dust devil could have travelled while appearing to be in the same position in the parallax images. The error in recorded time between image pairs was taken to be one second. Hence we extracted error estimates for the speeds of each dust devil. Errors on speed were large when (i) dust devils were moving towards or away from the spotters (as most of the uncertainty in position is radial) and (ii) when distant dust devils were moving perpendicular to the spotters' look direction. Both of these effects were exacerbated by the effects of a small time between adjacent image pairs (this was sometimes as small as five seconds, or a 20% uncertainty). Hence the estimated errors on the speed of the dust devils were sometimes as large as several tens of percent.

We use the meteorology data from 10 m height, for this is where simultaneous speed and direction measurements were made. For these data, any wind direction measurements that were

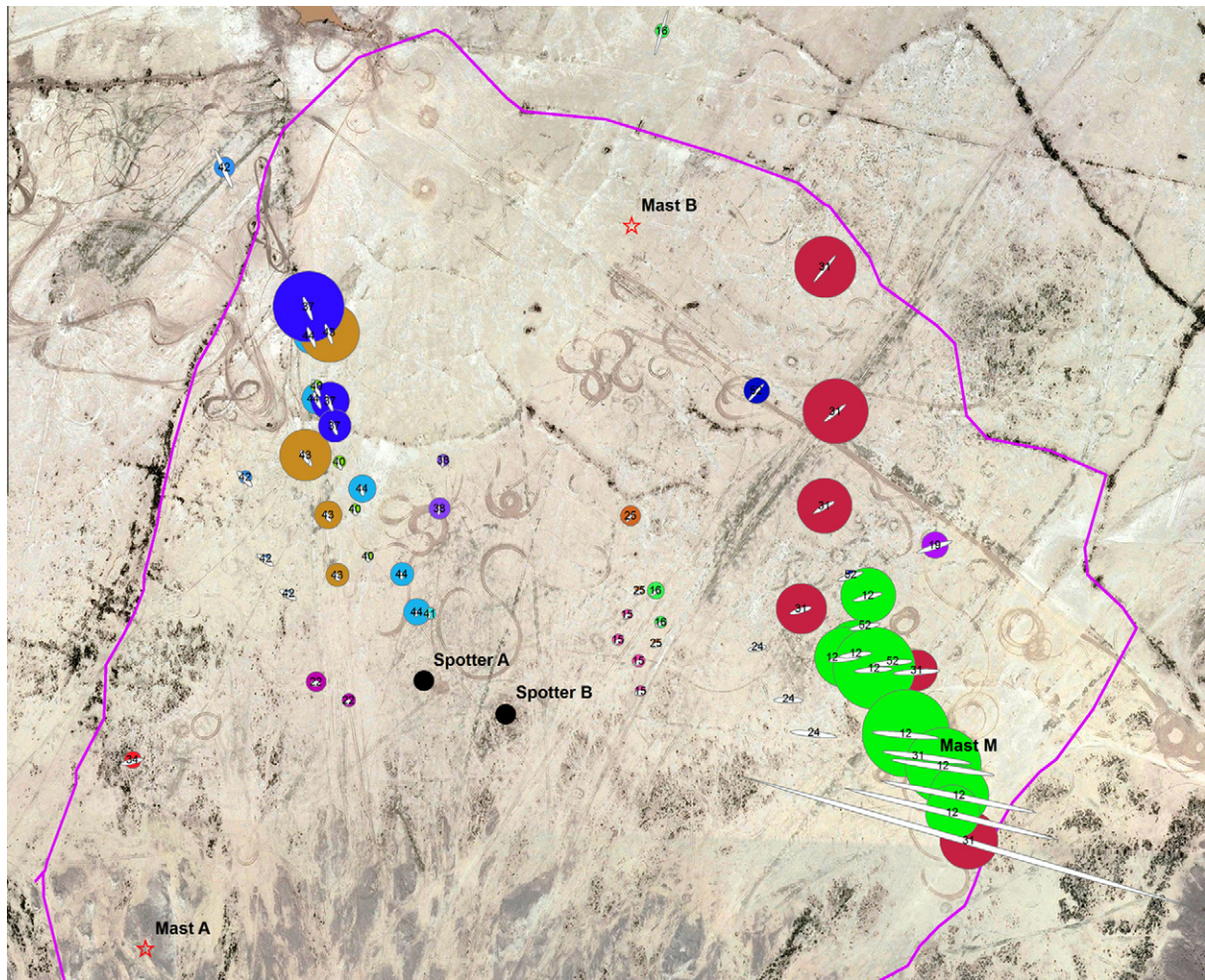


Fig. 4. GIS map view of the northern part of the Eldorado Valley study area showing positional error ellipses. Colored circles represent the location and size of individual dust devils during the field campaign day of the 23rd June 2010. Each dust devil is represented by a different color. The pale-colored ellipses represent the calculated uncertainty in the center point of each dust devil location. Note how the error in range gets very large for those dust devils co-aligned with the two spotter stations. (For interpretation of the references to color in this figure legend, the reader is referred to the web version of this article.)

made when wind speeds were less than 0.9 ms^{-1} were removed from all calculations. This is necessary because this is the threshold wind speed required to move the wind vanes, so very low wind speeds give fallacious direction data.

We compared the ambient wind data with the dust devil ground velocity vectors in several ways in order to compare different temporal and spatial scales of dependence on ambient winds. First, we used only those times of day when each dust devil image pair was acquired to define a time period for that specific dust devil ground-track section. The position of the dust devil at the center of this track-section was then used to determine which of the two meteorology masts (A or B) was nearest during that time. For each dust devil track section velocity vector, we compared those wind vector data from the nearest mast within that time period. This comparison investigates whether dust devil ground motion is related to ambient wind speed at the smallest spatial and temporal scales. Secondly, we used a 20 min rectangular window function to smooth the ambient wind data and then compared the dust devil ground speeds from individual ground tracks with the smoothed data from the nearer mast. This removes short timescale variations in ambient wind, but still compares individual dust devil ground speeds with the winds at the nearer mast. Thirdly, we averaged all the dust devil ground velocities each day over three 2-h periods: 10:00–12:00, 12:00–14:00 and 14:00–16:00 and compared these with the mean ambient wind velocities measured over this time.

This comparison investigates whether dust devil motions are representative of ambient winds measured at the scale of the study area ($\sim 1 \text{ km}$ linear dimensions) and provides several measurements over the course of a dust devil active day (10:00–16:00). Finally, in order to compare daily dust devil motion and meteorology data, we averaged the mean ambient wind velocity across the whole of the dust devil active period of each day and compared these with day-averaged dust devil ground velocities.

5. Results

5.1. Track shape

Fig. 5 shows a summary of all the plotted tracks of dust devils observed during the 2009 Eloy and 2010 Eldorado Valley field campaigns. In each figure, different line symbologies represent different days in the study. It can easily be seen that the overall patterns of dust devil motion are West to East for Eloy and approximately South to North for Eldorado, although in each of the studies one day of anomalous path direction occurs. No attempt is made in this study to distinguish between large and small dust devils (although most of the dust devils observed here were at least a few meters in diameter and persisted for several tens of seconds or longer). Overall, most of the dust devils followed straight paths

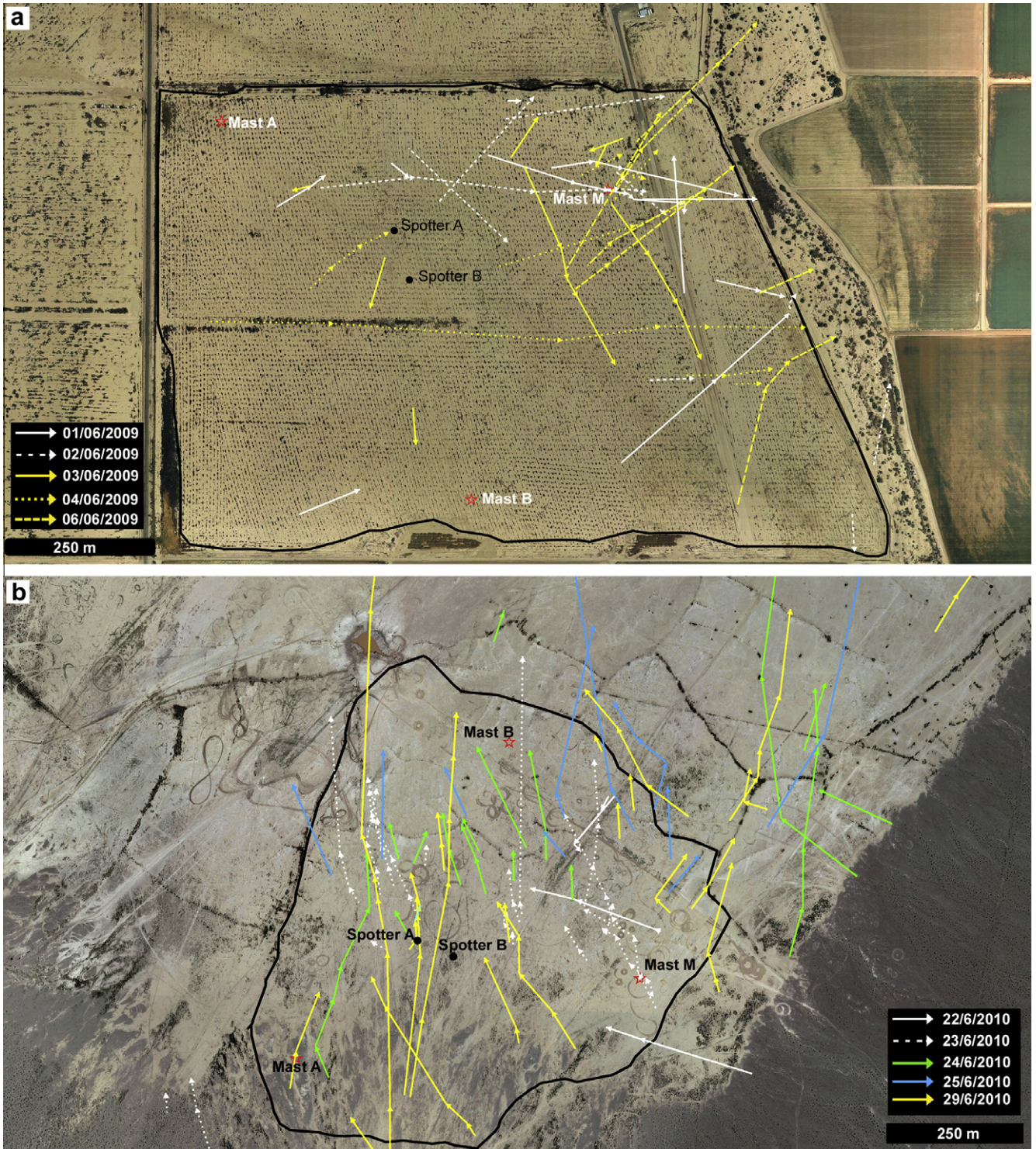


Fig. 5. Dust devil ground motion paths calculated from the imaging campaign in the Eloy (top) and Eldorado Valley (bottom) study areas. Each arrow head represents a separate track section; each composite line of several track sections represents a different dust devil.

on the 500 m scale. We did not observe curlicue paths as seen on Mars (e.g., Edgett and Malin, 2000) nor a majority of severely curved paths, as reported to be dominant on Earth (Flower, 1936).

5.2. Dust devil ground speed

Fig. 6 shows the calculated dust devil ground speed plotted against the mean ambient wind speed (measured at 10 m height

above the surface for the tower nearest to the dust devil). Each point represents an individual measurement based on two pairs of stereo spotter images; in Fig. 6a the mean wind speed was calculated for the time interval between these two pairs of images, and in Fig. 6b it was calculated using a 20 min rectangular window function. A linear least squares fit, un-weighted through the origin shows a relationship between dust devil ground speed and ambient wind speed, although the amount of scatter is large. The scatter

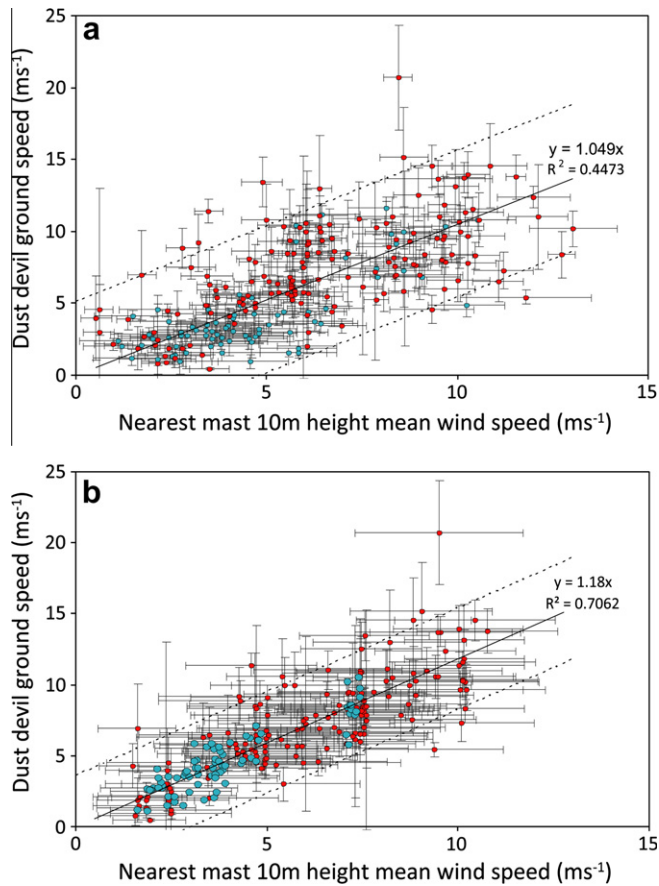


Fig. 6. All dust devil ground speeds plotted against ambient wind speed measured at 10 m height. The horizontal error bars represent one standard deviation of the wind speed data. The vertical error bars represent estimated uncertainty on the speed measurement as described in Section 4.3. Dashed lines in both plots indicate 95% prediction intervals on Y . Each data point represents a single dust devil ground track section, not a single dust devil. Blue points are Eloy data, red points are Eldorado Valley data. In (a) the ambient wind speed shown is extracted from the 1 Hz sampling rate wind speed data, averaged over the time the dust devil was active during that section of its track. In (b) the ambient wind speed shown is extracted from a 20 min rectangular window function applied to the 1 Hz wind data, centered on the time the dust devil was active. (For interpretation of the references to color in this figure legend, the reader is referred to the web version of this article.)

is much less when the instantaneous dust devil wind speed is compared to wind speed data that has been subjected to a 20 min rectangular smoothing window function. The linear fit suggests that dust devil forward velocity appears to be about 5–15% faster than the 10 m height wind speeds as measured from the nearest meteorology mast. Within uncertainty limits, both Eloy and Eldorado data plot on the same best fit line, so regression lines shown in Fig. 6 are fitted to both data sets.

Fig. 7 shows wind speed data averaged spatially and temporally. In Fig. 7a dust devil ground speed and ambient wind speed are averaged over 2-h periods, so each point represents the mean dust devil ground speed for that time period for that day. The data for dust devil ground speed are averaged over the entire study area. Results from both study areas are shown on the same graph. An obvious outlier to the data can be seen in Fig. 7a, this point representing a single, fast-moving dust devil observed at Eldorado Valley during the afternoon of 25/6/2010. Several fast moving dust devils were seen at this time; this was the windiest day of the ten field days described here.

Fig. 7b shows similar data, but averaged over a whole day (10:00–16:00). The daily and two-hourly averaged data show sim-

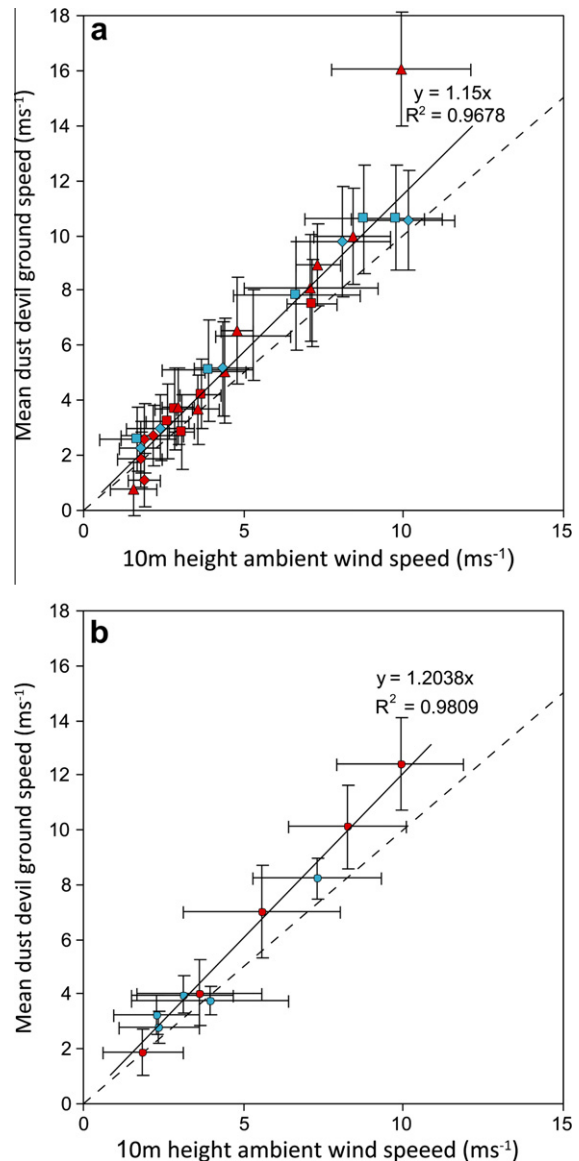


Fig. 7. Time averaged dust devil ground speed plotted against ambient wind speed. (a) Shows both dust devil ground speed and 10 m height ambient wind speed averaged over three 2-h periods per day. Diamonds represent data for the 10:00–12:00 period, squares for 12:00–14:00 and triangles 14:00–16:00. Filled symbols are for Eloy, unfilled for Eldorado Valley. Horizontal error bars represent the standard deviation of the ambient wind speed data. Vertical error bars represent the average percentile error on the ground speed from those dust devil tracks within that time period. Note that the outlier data point, top-right, is excluded from the best-fit. (b) Shows the same data but averaged over a whole day (10:00–16:00). Blue symbols are for Eloy, red for Eldorado Valley. In both plots, the dashed line shows the 1:1 ratio between dust devil ground speed and ambient wind speed for comparison. (For interpretation of the references to color in this figure legend, the reader is referred to the web version of this article.)

ilar results: a strong correlation between dust devil ground speed and ambient wind speed. In both cases, the dust devil ground speed is consistently faster than the ambient wind speed measured at 10 m height. The data show that both ambient wind speed and dust devil ground speed were on average slightly faster at the Eldorado Valley field site than the Eloy site.

5.3. Dust devil ground motion direction

Ambient wind direction data were compared to the time averaged dust devil azimuth data at both daily (Fig. 8a) and 2-h time

scales (Fig. 8b). This was done because there was some morning to afternoon variability in direction of the ambient winds, especially on those days with lower wind speed. Hence we were able to test whether dust devil ground direction followed this variation. For the 2-h averaged data, the difference between the mean ambient wind direction and the mean dust devil motion direction during that time was calculated, giving direction difference values in the range -180° to $+180^\circ$. Here, positive values represent an ambient wind direction that is clockwise (i.e., to the right hand side) of the dust devil track azimuth, and negative values counter-clockwise. Track data from 2-h periods with only one measurement were excluded from the comparison. Fig. 8b shows these data for

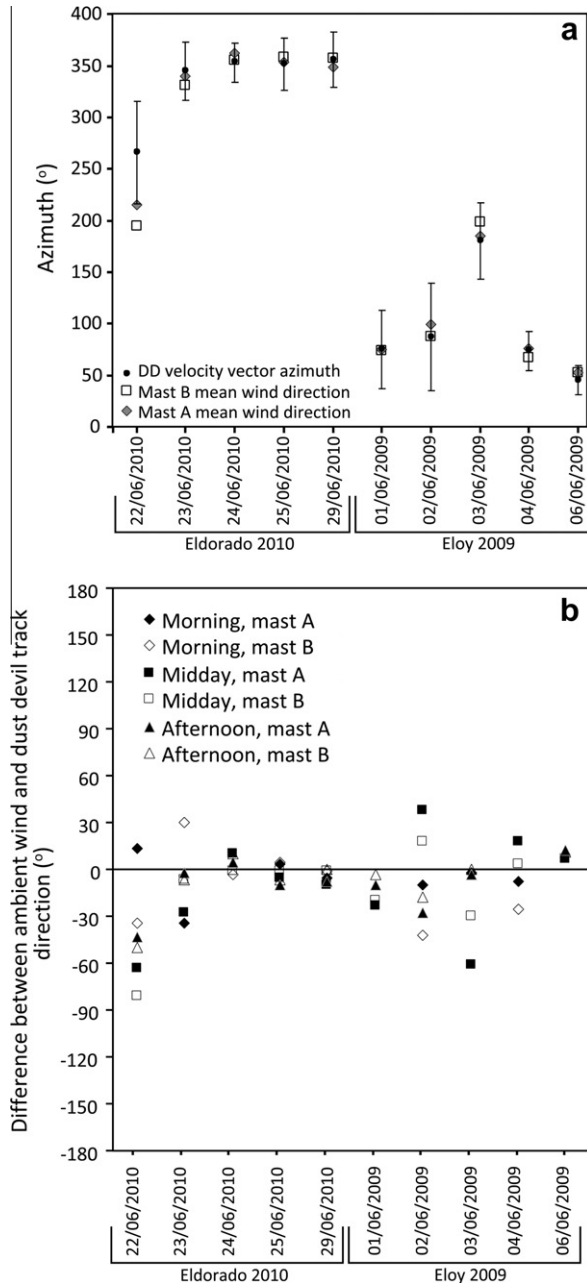


Fig. 8. Time-averaged ambient wind speed measurements compared with time-averaged dust devil ground directions. (a) Presents 2-h averaged data and shows the difference between the dust devil track azimuth and the 10 m height wind direction. The vertical error bars show 1 standard deviation in the dust devil ground velocity direction data. (b) Shows day-averaged ambient wind directions (at 10 m height) and daily mean dust devil ground velocity azimuths. The mean values presented are vector averages.

the 10 field days, broken down by time of day. The difference between the direction of the time-averaged dust devil ground velocity and the direction of the 10 m height ambient wind is less than 90° in all instances, and only 9 out of 52 measurements show a difference of more than 30° . There is no consistent deviation to one side or the other of dust devil ground motion direction compared to the ambient wind direction.

Fig. 8a shows day-averaged dust devil ground motion direction plotted against day-averaged wind direction (10:00–16:00 local time) for each of the ten study days. In all cases except one, the mean wind direction was very close to the mean dust devil ground motion direction (usually differing by less than 10° , and certainly within one standard deviation). The only day with a larger disparity was the 22nd June in 2010; this day had the lowest mean ambient wind speeds (Table 1).

Lower wind speed days in general have more variability in dust devil track ground direction. Fig. 9 shows standard deviation of day-averaged dust devil ground motion direction as a function of day-averaged wind speed (averaged over both masts). The days with mean speeds of less than about 3 ms^{-1} had much greater variability in dust devil ground motion direction than those from faster wind days. Table 1 shows a summary of the wind speed and direction data and comparison with the dust devil ground velocity. The mean ambient wind speeds presented are averages of the 1 Hz sample rate data at 10 m height limited to the dust devil active periods (10:00–16:00 local time). Both Mast A and B data are shown.

5.4. Dust devil diameter

To test whether dust devil ground speeds are a function of diameter, we extracted the measured diameters of each dust devil from the single day with the most dust devil measurements (29th June 2010; Eldorado Valley). A single day's data was used, to somewhat exclude the effects of ambient wind strength (the 20 min smoothed wind speed from this day had only a narrow range: from $\sim 5 \text{ ms}^{-1}$ in the morning, to $\sim 7 \text{ ms}^{-1}$ in the afternoon). Dust devil diameter was obtained by averaging the diameter from the image pair taken at the beginning and end of each ground track, giving a total of about 60 measurements of diameter and ground speed (Fig. 10). There was no correlation between dust devil size and ground speed. We also calculated the difference between dust devil ground speed and ambient wind speed (at 10 m height, measured at the nearest meteorology mast) for each track section. This was done to examine whether the dust devil ground speed in this track section was faster or slower than the ambient winds during this period, and if this was influenced by diameter. Again, there was no correlation between dust devil size and dust devil ground speed relative to ambient wind speed. We conclude that dust devil ground velocity is independent of dust devil diameter.

5.5. Results summary

The key results are: (i) In general, dust devil ground velocity is a function of ambient wind velocity as measured at 10 m height. Ground speed is 10–20% higher than ambient wind speed recorded at 10 m height; (ii) Measurements of individual dust devil ground velocities give an approximate indication of the instantaneous local (within a few 100 m) wind velocity at 10 m height. Much better correlation is seen in the 2-h and day-averaged speed and direction data; (iii) Almost all the dust devils recorded here tend to have linear to curvilinear tracks, rather than following sinuous or curlicue paths; (iv) There is no indication that a dust devil's ground velocity is related to its diameter.

Table 1
Mean wind speed, azimuth and dust devil ground velocity summary. Data for dust devil ground speed (V) and azimuth are averaged over all dust devil tracks measured during that day. Ambient wind speed (W) and azimuth are averaged over the dust devil active portion of the day (11:00–16:00 local time). EV = Eldorado Valley, EL = Eloy. One standard deviation values (Δ) are given for mean dust devil ground speed and direction.

Site	Date	DD mean V (m/s)	Δ DD mean V (m/s)	DD azimuth ($^{\circ}$)	Δ DD azimuth ($^{\circ}$)	Ambient mean W , Mast A (m/s)	Ambient mean W , Mast B (m/s)	Ambient mean wind direction, Mast A ($^{\circ}$)	Ambient mean wind direction, Mast B ($^{\circ}$)
EV	22 June 2010	2.3	1	266	50	1.8	1.9	215	195
EV	23 June 2010	5.55	1.31	345	28	3.6	3.7	340	331
EV	24 June 2010	10.25	1.55	353	19	7.8 ^a	8.7	2 ^a	356
EV	25 June 2010	11.85	1.6	352	25	9.6	10.2	354	358
EV	29 June 2010	7.2	1.7	356	27	5.2	6	349	357
EL	01 June 2009	3.52	0.52	75	38	3	3.2	75	74
EL	02 June 2009	1.96	0.28	87	52	2.3	2.3	99	88
EL	03 June 2009	2.84	0.26	180	37	2.3	2.4	185	199
EL	04 June 2009	3.88	0.45	74	19	4.1	3.8	76	67
EL	06 June 2009	9.00	1.21	45	14	7.5	7.1	53	53

^a Due to equipment failure, data were collected only from 13:11 to 16:00 on this day.

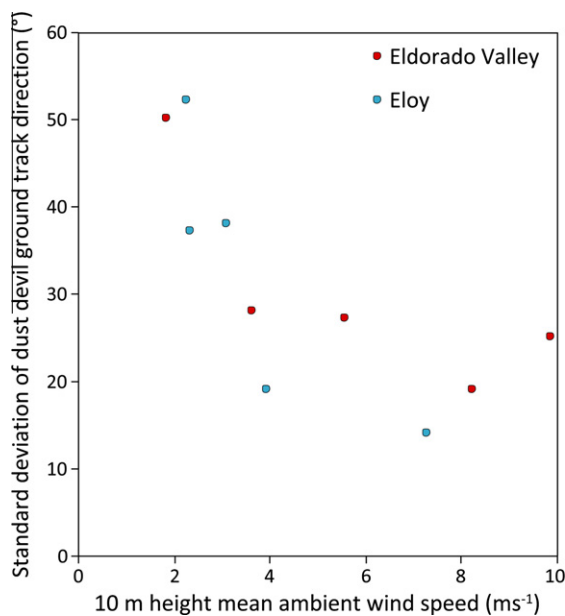


Fig. 9. Standard deviation of dust devil ground motion direction with mean daily 10 m height wind speed. Each point shows a different day.

6. Discussion

The data provided show that dust devils tend to move with the ambient wind field. This is not an unexpected result given previous observations (Flower, 1936; Crozier, 1970). What is unexpected, though, is that the dust devil motion is so fast: daily mean forward speeds of up to 12 ms^{-1} were recorded. Interestingly, the dust devil translational speeds found in this study are similar in magnitude to 15 measurements of dust devil ground speed made by Crozier (1970) who also used a stereo imaging system, but who only obtained estimates of ambient wind speed. Several previous studies that attempted to record dust devil forward motion concluded that dust devils travel slower than ambient wind speeds (e.g., Snow and McClelland, 1990). However, many of these have also been subjective, estimating dust devil position (and hence velocity) by reference to surface features, or have not presented reliable meteorology data. We suggest that our quantitative, long-baseline, stereo measurements of dust devil position are far more reliable than single viewpoint azimuth and range estimates, and hence our quantitatively-derived dust devil ground velocities are more reliable.

We found no evidence that the ground velocity of a dust devil is related to its diameter (Fig. 10). This agrees with remote sensing

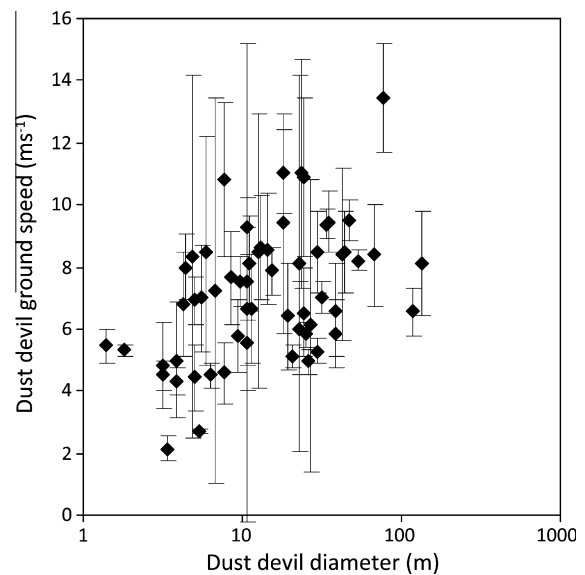


Fig. 10. Dust devil ground speed as a function of dust devil diameter, for approximately 60 dust devil measurements taken on 29th June 2010 in Eldorado Valley.

observations of martian dust devils (Stanzel et al., 2006, 2008; Reiss et al., 2011) but is somewhat at odds with observations from the ground; Greeley et al. (2010) find some evidence for smaller dust devils travelling faster. We note that there seems to be no reason why dust devil diameter should affect velocity, because dust devils are not removed from the local wind regime, but occur within it. Hence a larger diameter dust devil would move at a speed that is representative of a slightly larger range of horizontal positions in the background wind, but this would not have any net effect on the mean velocity we also found no evidence for consistently curved or curlicue tracks, unlike early observation of dust devils on Earth (Flower, 1936). However, the longest tracks we documented were about a kilometer in length, and most were only a few 100 m long, so it is possible that longer track observations (or a higher sampling rate) might provide a different result.

In this study, the time-averaged dust devil ground speeds are consistently $>10\%$ faster than the time-averaged boundary layer wind speed measured at 10 m height. It seems very unlikely that this could be caused by spatial inhomogeneities in the wind field (for example due to the position of the masts resulting in their measuring preferentially low wind speeds) as the trend is consistent across five days per study area and across two different study areas. We conclude that the dust devils are travelling faster than

the winds measured at 10 m height, and instead travel at a similar speed to the boundary layer winds at a height above 10 m. This height can be calculated assuming a simple boundary layer wind velocity profile such as

$$\frac{U}{u} = \frac{1}{0.4} \ln \frac{z}{z_0} \quad (1)$$

where U is the wind speed at height z , u^* is the surface friction wind speed and z_0 the aerodynamic roughness. We can approximate the height at which dust devil translation speed equates to the ambient wind speed. Assuming a value for z_0 of 0.001 m, consistent with measurements of the playa in Eldorado Valley (Metzger, 1999), and that at 10 m height the dust devil translation speed is 10% greater than the boundary layer wind speed, Eq. (1) suggests that the height at which the boundary layer wind speed is 10% faster than its 10 m value is ~ 25 m. For values of z_0 an order of magnitude smaller and larger (i.e., 0.0001 m or 0.01 m), the heights at which the boundary layer wind speed is 10% greater than its 10 m value are ~ 20 m and ~ 30 m. This shows that the calculated height is relatively insensitive to the value of z_0 .

The simple calculation for the height suggests that dust devils travel at a speed equivalent to ambient winds within the planetary boundary layer about 20–30 m above the surface. This in turn suggests that the base of a dust devil is travelling faster than the time-averaged boundary layer winds near the ground and demonstrates that dust devils contain intense near-surface winds of several tens of meters per second. We suggest that this is because dust devils are strong, highly nonlinear phenomena which are able to maintain their vertical coherence and move at the same velocity at almost all heights, even in the presence of vertical shear in the background wind. This does not mean that the dust devil ground motion is only influenced by the wind at one height (20–30 m in this study), but that its motion must reflect both an integrated wind profile over its whole cross-section and the integrated effect of the frictional near-surface boundary layer. This reinforces the conclusion that dust devil wind shear alone is sufficient to lift most dust to granule-scale sediments on Earth (Balme et al., 2003), and that other mechanisms, such as the pressure-deficit suction effect (Balme and Hagermann, 2006) or electrification (Kok and Renno, 2006) are not required (although they may contribute). Whether this is also the case on Mars has not yet been tested.

In terms of direction, observed dust devil ground motions were consistently within about 30° of the direction of the 10 m height ambient winds. In particular, when dust devil ground motion direction was averaged over a whole day, the agreement between mean dust devil direction of travel and ambient wind direction is very close. Those days where there was less agreement were also those days with the lowest values of ambient wind speed (Fig. 9), suggesting unsurprisingly that at low speeds dust devils follow a more variable path. This might also be due to instrument effects, for wind direction data points obtained when wind speed was low were filtered out.

The measurements presented here suggest that, on Earth, dust devil ground velocity can be used as a proxy for measurements of ambient wind velocity in the boundary layer at 20–30 m above ground level. Single measurements of individual dust devils provide a reasonable approximation of the ambient wind speeds averaged over 20 min (Fig. 6b), but multiple measurements of several dust devils in the same local area give a more reliable indication of the mean wind field at this height over a several-hour period (Fig. 7).

If the agreement between dust devil ground motion and boundary layer wind velocity also holds true for Mars, and there seems no physical reason why this should not be the case, then multiple images of dust devils (from orbit or the surface) can be used to measure martian wind speeds and direction. Furthermore, even

single measurements of dust devil motion can provide an estimate of ambient wind speed within certain limits (for example, the spread of the data in Fig. 6). Preliminary studies in this direction have begun: Stanzel et al. (2008) found broad agreement between wind speeds from global climate models at heights equal to the top of observed dust devil and the ground speeds of the dust devils. The results presented here support this methodology, but it should be noted that although dust devils in a single HRSC image triplet are all observed within a few minutes of one another, spatially they can be fairly distant, as HRSC images can be tens of kilometers wide and hundreds of kilometers in latitudinal extent. Hence, these dust devils are not necessarily local to one another in quite the same way as those reported in this study for the Earth. Nevertheless, they do represent a snapshot of dust devil ground speed in this region and at this time. Overall, the HRSC data show that dust devil ground speeds on Mars appear to be about three times greater than observed on Earth, based on our study results. Greeley et al. (2010) find speeds more similar to those we measured on Earth, but examined much smaller dust devils, and used what is perhaps a much less accurate method to estimate position (and hence speed). We suggest that variations between dust devil ground speeds seen in different regions of Mars reflect the local wind conditions, and a larger catalogue of dust devil ground velocities should be developed. The Mars Science Laboratory *Curiosity* Rover should provide at least one more study area. Therefore, comparison between Earth and Mars can at present only be a preliminary estimate, for we report only two specific areas on Earth, and the dataset for Mars is also spatially limited.

The use of dust devils as proxies for wind speed within the boundary layer on Mars is important for several reasons. First, tracking dust devils provides a technique to measure wind speed that probes a part of the boundary layer (probably tens to hundreds of meters above ground level for Mars) that is difficult to sample for planetary missions: too high above the ground for meteorology sensors to be easily deployed, and too low for orbiting sounding instruments to view. This part of the boundary layer is also important as an input for climate models as many Mars global climate models have a lowest level about 5 m from the surface and two or three more levels up to about 100 m (e.g., Forget et al., 1999; Haberle et al., 1999; Lewis et al., 1999).

Second, our results potentially show that dust devil ground velocity is not micro-controlled by surface relief but by boundary layer winds. Hence, measurements of wind velocity derived from dust devil motion probably do not suffer from the effects of small surface obstacles, as might be the case for meteorology instruments on landing craft, which can be ‘shadowed’ by local topography, or suffer instrument breakdowns or miscalibration (e.g., Chamberlain et al., 1976; Murphy et al., 1990; Schofield et al., 1997). However, it should be noted that further field studies in dust devil active regions with more significant roughness elements are required to confirm this result, as both Eloy and Eldorado are relatively aerodynamically smooth.

Third, dust devil ground velocity can be derived for many locations and times across the martian surface, providing a large data set that is useful not only for understanding the climate but perhaps also for determining the environmental conditions and therefore safety of future landing sites. This technique also allows wind speeds to be extracted from past imaging data, and this can be used to help validate climate models over several Mars years.

To determine robustly whether dust devils can be used as proxies for wind velocity on Mars, and if so to calculate at what height within the boundary layer dust devil motions are representative of, will require more research, specifically using in situ observations from Mars and/or atmospheric modeling. For in situ sampling, multiple measurements of dust devil position, together with simultaneous, ambient wind speed/direction measurements from

a nearby landing craft, are required. Assuming that any meteorology mast on Mars will be at a relatively low height (1–2 m), a reliable measurement of local surface friction roughness must then also be obtained if boundary layer wind speeds are to be extrapolated to higher levels. Using these data, dust devil ground velocities could then be compared with ambient wind data. If there appears to be a linear relationship between ambient wind velocity and dust devil ground motion, then the level within the boundary layer at which the dust devil motion is representative of can be extrapolated from knowledge of the surface friction roughness. This method could be attempted by *Curiosity*, which has both surface imaging (Malin et al., 2010) and meteorology instruments (Gómez-Elvira et al., 2011), or by the proposed ESA ExoMars mission.

Error in estimating the dust devil velocity on Mars could be large, however, because dust devil position will have to be estimated based on comparison with surface features, not long baseline stereo imaging, although some very reliable data might be obtained by simultaneous targeted orbital imaging. Also, measurements of surface friction roughness could be challenging to obtain with the meteorology instruments that are to be deployed, although we note that new global-scale estimates of aerodynamic roughness length based on rock abundances have been recently derived (Hébrard et al., 2012).

In-situ measurements could be complemented by the use of high-resolution numerical modeling techniques. Recent work has demonstrated that convective vortices can be resolved in both martian and terrestrial simulations (Kanak et al., 2000; Michaels and Rafkin, 2004; Spiga and Forget, 2009). Such models can be validated for Earth using the relatively plentiful field observations such as those presented here, and then could provide a means to investigate how dust devil ground velocity might vary with changing planetary parameters to those appropriate to Mars and thus to establish the relationship between dust devil velocity and ambient wind profile on Mars.

Finally, although the methodology presented here has provided a large amount of reliable data for dust devil ground velocities, specific aspects of the method proved time consuming, so there is scope for some improvement, especially with a larger budget. One specific improvement would be to use three fixed cameras with higher-specification optics and larger sensors, set in an inward-looking, triangular arrangement. Although this would be expensive if equivalent angular resolution was to be maintained for the same study area size (i.e. cameras with larger sensors and better optics would be required), it would mean that registration of the images against a background would not be necessary, hence saving one step in the image processing pipeline. This system would also mean that all three cameras could be operated remotely by a single spotter, so it might also be a more efficient field approach.

7. Conclusions

Using long baseline stereo imaging we have measured the precise size and location of many dust devils over two field seasons. We have used multiple images of the same dust devil to calculate the ground velocity of each dust devil and compared this to ambient wind velocity. The methodology has been successful, and demonstrates the utility of this approach.

Day and 2-h averaged dust devil ground speed correlates well with ambient wind speeds averaged over the same period measured at 10 m height. Individual measurements of dust devil ground speed match instantaneous measurements of ambient wind speed more poorly, but are better approximated by a 20-min smoothing window applied to ambient wind speed data. Dust

devil ground velocity direction also closely matches the ambient wind direction. In general, dust devils appear to travel 10–20% faster than ambient wind speed measured at 10 m height, suggesting that dust devils ground speed are representative of the boundary layer wind speeds at heights of a few tens of meters above ground level.

That dust devils move faster than the time-averaged near-surface wind field demonstrates that the near-surface winds associated with dust devils are intense. This is consistent with the notion that surface shear stresses caused by dust devils are high enough to entrain the material seen within them, rather than necessitating other mechanisms for dust lifting based on pressure deficit or electrical charging. This might not be the case on Mars.

Given the link between ambient wind speed and dust devil ground velocity on Earth, it seems likely that a similar one should apply on Mars. Determining the details of this relationship would likely require new in situ or modeling studies but, if completed successfully, could provide a quantitative method for dust devils on Mars to be used as proxies for wind speed measurements. Such data would be very useful inputs for climate models and for determining the state of the atmosphere during landing site studies.

Acknowledgments

This work was funded by the NASA Mars Fundamental Research Programme, Grant No. NNX08AP32G. This is Planetary Science Institute contribution number 596. We thank Patrick Whelley and Dennis Reiss for instructive reviews that helped to improve the paper.

References

- Balme, M.R., Greeley, R., 2006. Dust devils on Earth and Mars. *Rev. Geophys.* 44. <http://dx.doi.org/10.1029/2005RG000188>.
- Balme, M.R., Hagermann, A., 2006. Particle lifting at the soil–air interface by atmospheric pressure excursions in dust devils. *Geophys. Res. Lett.* 33, L19S01. <http://dx.doi.org/10.1029/2006GL026819>.
- Balme, M.R., Metzger, S.M., Towner, M.C., Ringrose, T.J., Greeley, R., Iversen, J.D., 2003. Friction wind speeds in dust devils: A field study. *Geophys. Res. Lett.* 30. <http://dx.doi.org/10.1029/2003GL017493>.
- Cantor, B.A., Kanak, K.M., Edgett, K.S., 2006. Martian dust devils, and their tracks, as recorded by the Mars Global Surveyor Mars Orbiter Camera, September 1997–January 2006. *J. Geophys. Res.* 111, E12002. <http://dx.doi.org/10.1029/2006JE002700>.
- Chamberlain, T.E., Cole, H.L., Dutton, R.G., Greene, G.C., Tillman, J.E., 1976. Atmospheric measurements on Mars – The Viking meteorological experiment. *Bull. Am. Astron. Soc.* 57, 1094–1104.
- Crozier, W.D., 1970. Dust devil properties. *J. Geophys. Res.* 75, 4583–4585.
- Edgett, K.S., Malin, M.C., 2000. New views of Mars eolian activity, materials, and surface properties: Three vignettes from the Mars Global Surveyor Orbiter camera. *J. Geophys. Res.* 105, 1623–1650.
- Ellehoj, M.D. et al., 2010. Convective vortices and dust devils at the Phoenix Mars mission landing site. *J. Geophys. Res. E: Planets* 115. <http://dx.doi.org/10.1029/2009JE003413>.
- Ferri, F., Smith, P.H., Lemmon, M.T., Renno, N.O., 2003. Dust devils as observed by Mars Pathfinder. *J. Geophys. Res.* 108. <http://dx.doi.org/10.1029/2000JE001421>.
- Fisher, J.A. et al., 2005. A survey of martian dust devil activity using Mars Global Surveyor Mars Orbiter Camera images. *J. Geophys. Res.* 110. <http://dx.doi.org/10.1029/2003JE002165>.
- Flower, W.D., 1936. Sand devils. *Lon. Met. Off. Prof. Notes* 5, 1–16.
- Forget, F. et al., 1999. Improved general circulation models of the martian atmosphere from the surface up to above 80 km. *J. Geophys. Res.* 104, 24,155–24,175.
- Gómez-Elvira, J. et al., 2011. Rover environmental monitoring station for MSL mission. In: Fourth International Workshop on the Mars Atmosphere: Modelling and Observations, Pierre and Marie Curie University, Paris, pp. 473–476.
- Greeley, R. et al., 2003. Martian dust devils: Laboratory simulations of particle threshold. *J. Geophys. Res.* 108. <http://dx.doi.org/10.1029/2002JE001987>.
- Greeley, R. et al., 2006. Active dust devils in Gusev crater, Mars: Observations from the Mars Exploration Rover Spirit. *J. Geophys. Res.* 111. <http://dx.doi.org/10.1029/2006JE002743>.
- Greeley, R. et al., 2010. Gusev crater, Mars: Observations of three dust devil seasons. *J. Geophys. Res.* 115. <http://dx.doi.org/10.1029/2010JE003608>.

- Haberle, R.M. et al., 1999. General circulation model simulations of the Mars pathfinder atmospheric structure investigation/meteorology data. *J. Geophys. Res.* 104, 8957–8974.
- Hébrard, E. et al., 2012. An aerodynamic roughness length map derived from extended martian rock abundance data. *J. Geophys. Res.* 117. <http://dx.doi.org/10.1029/2011JE003942>.
- Ives, R.L., 1947. Behavior of dust devils. *Bull. Am. Meteorol. Soc.* 28, 168–174.
- Kanak, K.M., 2005. Numerical simulation of dust devil-scale vortices. *Q. J. R. Meteorol. Soc.* 131, 1271–1292.
- Kanak, K.M., Lilly, D., Snow, J.T., 2000. The formation of vertical vortices in the convective boundary layer. *Q. J. R. Meteorol. Soc.* 126, 2789–2810.
- Kok, J.F., Renno, N.O., 2006. Enhancement of the emission of mineral dust aerosols by electric forces. *Geophys. Res. Lett.* 33. <http://dx.doi.org/10.1029/2006GL026284>.
- Lewis, S.R. et al., 1999. A climate database for Mars. *J. Geophys. Res.* 104, 24,177–24,194.
- Malin, M.C., Edgett, K.S., 2001. Mars Global Surveyor Mars Orbiter Camera: Interplanetary cruise through primary mission. *J. Geophys. Res.* 106, 23,429–23,570.
- Malin, M. C. et al., 2010. The Mars Science Laboratory (MSL) mast-mounted cameras (Mastcams) flight instruments. *Lunar Plan. Sci.* XLI, Abstract 1123.
- Metzger, S.M., 1999. Dust devils as aeolian transport mechanisms in southern Nevada and in the Mars Pathfinder landing site. PhD, Univ. Nevada, Reno.
- Metzger, S.M., Carr, J.R., Johnson, J.R., Parker, T.J., Lemmon, M.T., 1999. Dust devil vortices seen by the Mars Pathfinder camera. *Geophys. Res. Lett.* 26, 2781–2784.
- Michaels, T.I., 2006. Numerical modeling of Mars dust devils: Albedo track generation. *Geophys. Res. Lett.* 33. <http://dx.doi.org/10.1029/2006GL026268>.
- Michaels, T.I., Rafkin, S.C.R., 2004. Large eddy simulation of atmospheric convection on Mars. *Q. J. R. Meteorol. Soc.* 128, 1–25.
- Murphy, J.R., Leovy, C.B., Tillman, J.E., 1990. Observations of martian surface winds at the Viking Lander 1 site. *J. Geophys. Res.* 95, 14,555–14,576.
- Neukum, G., Jaumann, R., 2004. HRSC: The high resolution stereo camera of Mars express. In: Wilson, A. (Ed.), *Mars Express: The Scientific Payload*. ESA SP-1240. ESA Publications Division, Noordwijk, pp. 17–35.
- Newman, C.E., Lewis, S.R., Read, P.L., Forget, F., 2002. Modeling the martian dust cycle, 1. Representations of dust transport processes. *J. Geophys. Res.* 107. <http://dx.doi.org/10.1029/2002JE001910>.
- Pathare, A.V., Balme, M.R., Metzger, S.M., Spiga, A., Towner, M.C., Renno, N.O., Saca, F., 2010. Assessing the power law hypothesis for the size-frequency distribution of terrestrial and martian dust devils. *Icarus* 209, 851–853.
- Reiss, D., Zanetti, M., Neukum, G., 2011. Multitemporal observations of identical active dust devils on Mars with the High Resolution Stereo Camera (HRSC) and Mars Orbiter Camera (MOC). *Icarus* 215, 358–369.
- Renno, N.O., Burkett, M.L., Larkin, M.P., 1998. A simple thermodynamical theory for dust devils. *J. Atmos. Sci.* 55, 3244–3252.
- Renno, N.O. et al., 2004. MATADOR 2002: A pilot field experiment on convective plumes and dust devils. *J. Geophys. Res.* 109. <http://dx.doi.org/10.1029/2003JE002219>.
- Ryan, J.A., Lucich, R.D., 1983. Possible dust devil vortices on Mars. *J. Geophys. Res.* 88, 11005–11011.
- Schofield, J.T. et al., 1997. The Mars Pathfinder atmospheric structure investigation meteorology (ASI/MET) experiment. *Science* 278, 1752–1758.
- Sinclair, P.C., 1969. General characteristics of dust devils. *J. Appl. Meteorol.* 8, 32–45.
- Snow, J.T., McClelland, T.M., 1990. Dust devils at white-sands-missile-range, New-Mexico. 1. Temporal and spatial distributions. *J. Geophys. Res.* 95, 13707–13721.
- Spiga, A., Forget, F., 2009. A new model to simulate the martian mesoscale and microscale atmospheric circulation: Validation and first results. *J. Geophys. Res.* 114. <http://dx.doi.org/10.1029/2008JE003242>.
- Stanzel, C., Pätzold, M., Greeley, R., Hauber, E., Neukum, G., 2006. Dust devils on Mars observed by the High Resolution Stereo Camera. *Geophys. Res. Lett.* 33. <http://dx.doi.org/10.1029/2006GL025816>.
- Stanzel, C., Pätzold, M., Williams, D.A., Whelley, P.L., Greeley, R., Neukum, G., H.C.-I.T., 2008. Dust devil speeds, directions of motion and general characteristics observed by the Mars Express High Resolution Stereo Camera. *Icarus* 197, 39–51.
- Thomas, P.C., Gierasch, P.J., 1985. Dust devils on Mars. *Science* 230, 175–177.
- Toigo, A.D., Richardson, M.L., Ewald, S.P., Gierasch, P., 2003. Numerical simulation of martian dust devils. *J. Geophys. Res.* 108. <http://dx.doi.org/10.1029/2002JE002002>.
- Towner, M.C., 2009. Characteristics of large martian dust devils using Mars odyssey thermal emission imaging system visual and infrared images. *J. Geophys. Res. E: Planets* 114. <http://dx.doi.org/10.1029/2008JE003220>.
- Williams, N.R., 1948. Development of dust whirls and similar small-scale vortices. *Bull. Am. Meteorol. Soc.* 29, 106–117.